BBA - Bioenergetics 1860 (2019) 350–359

Contents lists available at ScienceDirect

BBA - Bioenergetics

journal homepage: www.elsevier.com/locate/bbabio

A highly efficient heptamethine cyanine antenna for photosynthetic Reaction Center: From chemical design to ultrafast energy transfer investigation of the hybrid system

Simona la Gatta[a,b], Francesco Milano[b], Gianluca M. Farinola[a], Angela Agostiano[a,b], Mariangela Di Donato[c,d], Andrea Lapini[c,d], Paolo Foggi[c,d,e], Massimo Trotta[b,*], Roberta Ragni[a,*]

[a] Dipartimento di Chimica, Università degli Studi di Bari "Aldo Moro", Via Orabona 4, 70125 Bari, Italy
[b] CNR-IPCF, Institute for Physical and Chemical Processes, Bari unit, Via Orabona 4, 70125 Bari, Italy
[c] LENS (European Laboratory for Nonlinear Spectroscopy), via N. Carrara 1, 50019 Sesto Fiorentino, FI, Italy
[d] INO (Istituto Nazionale di Ottica), Largo Fermi 6, 50125 Firenze, Italy
[e] Department of Chemistry, University of Perugia, via Elce di Sotto 8, 06100 Perugia, Italy

ARTICLE INFO

Keywords:
Photoenzyme
Photosynthetic bacteria
Light harvesting antenna
Bioconjugation
Solar energy conversion
Photocurrent
Biophotovoltaic

ABSTRACT

The photosynthetic Reaction Center (RC) from the purple bacterium *Rhodobacter sphaeroides* has unique photoconversion capabilities, that can be exploited in assembly biohybrid devices for applications in solar energy conversion. Extending the absorption cross section of isolated RC through covalent functionalization with ad-hoc synthesized artificial antennas is a successful strategy to outperform the efficiency of the pristine photoenzyme under visible light excitation. Here we report a new heptamethine cyanine antenna that, upon covalent binding to RC, forms a biohybrid (hCyN7-RC) which, under white light excitation, has doubled photoconversion efficiency versus the bare photoenzyme. The artificial antenna hCyN7 successfully meets appropriate optical properties, i.e. peak position of absorption and emission maximum in the visible and NIR region respectively, large Stokes shift, and high fluorescence quantum yield, required for improving the efficiency of the biohybrid in the production of the charge-separated state in the RC. The kinetics of energy transfer and charge separation of hCyN7-RC studied via ultrafast visible and IR spectroscopies are here presented. The antenna transfers energy to RC chromophores within < 10 ps and the rate of Q_A reduction is doubled compared to the native RC. These experiments further demonstrate hCyN7-RC, besides being an extremely efficient white light photoconverter, fully retains the charge separation mechanism and integrity of the native RC photoenzyme, thus allowing to envisage its suitability as biohybrid material in bioinspired systems for solar energy conversion.

1. Introduction

Highly efficient photoactive systems converting visible light into chemical and electrical energy represent an active research field spurred by the need of renewable energetic sources and by the search of innovative materials with technological applications in various fields, including photovoltaics, sensing and photocatalysis. Biohybrid photoactive systems based on photoenzymes obtained from photosynthetic organisms are possible candidates versus non biological counterparts, in view of their extremely high efficiency (~100%) in promoting electron transfer processes upon photon absorption. In recent years it has been clearly demonstrated that biohybrid photoactive systems based on natural photoenzymes obtained from photosynthetic organisms could outperform the solar conversion capacity of the pristine photoenzymes [1–6]. This concept was further extended to different possible applications ranging from the generation of photocurrents to possible biotechnological applications of the whole photosynthetic organisms [7].

The design of biohybrids is inspired to the architecture and functioning of the photosynthetic apparatus of the *Rhodobacter* (*R.*) *sphaeroides* bacterium, that represents the simplest model system, composed by two antenna proteins, the light harvesting complexes LH1 and LH2, and a central photochemical core, the enzyme called reaction center (RC, Fig. 1). RC is a membrane-spanning protein enclosing nine non-covalently bound cofactors organized in two branches (A and B): starting from the periplasmic side, depicted in the top of Fig. 1, there are four bacteriochlorophylls (B), two of which forming a functional dimer that acts as a primary electron donor (P), two

* Corresponding authors.
E-mail addresses: massimo.trotta@cnr.it (M. Trotta), roberta.ragni@uniba.it (R. Ragni).

https://doi.org/10.1016/j.bbabio.2019.01.009
Received 3 July 2018; Received in revised form 11 December 2018; Accepted 26 January 2019
Available online 02 February 2019
0005-2728/

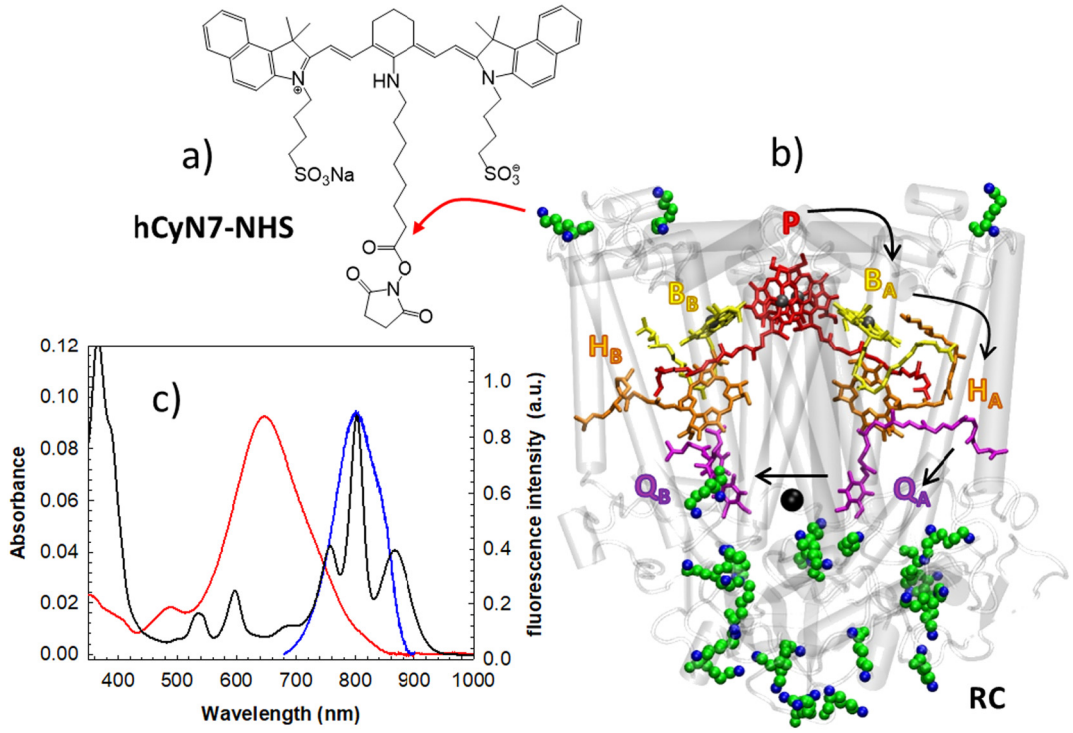

Fig. 1. a) Chemical structure of the hCyN7-NHS organic antenna sketched in close proximity to the residue lysine M110 which was found to be one of the most accessible residues for RC bioconjugation [13]. b) Schematic drawing of the RC (PDB ID: 1AIJ [14]) of *R. sphaeroides* bacterium with nine cofactors in the A and B branches. The lysine residues targets for the bioconjugation reaction are drawn as van der Waals spheres (carbon in green and nitrogen in blue). c) Optical absorption spectra of the RC (black), hCyN7 (red), and emission spectrum of hCyN7 (blue). The absence of carotenoid molecule bound to the RC in the strain R26 makes this mutant more suitable for our investigation because its optical spectrum is simpler than the wild type one lacking the intense absorption peaks of the carotenoids. (For interpretation of the references to colour in this figure legend, the reader is referred to the web version of this article.)

bacteriopheophytins (H) and two quinone (Q) molecules acting as primary (Q_A) and secondary (Q_B) electron acceptors, respectively. A non-heme Fe^{2+} ion is found in between the quinones. The electron generated by the absorption of a photon is shuttled along branch A and reaches the final acceptor Q_B within 100 µs. The resulting charge-separated state, or hole-electron couple, $P^+Q_B^-$ has a lifetime in the range of seconds that depends on the surrounding environment [8,9]. If the Q_B-binding site is empty or inhibited, the charge-separated state involves the primary electron acceptor and the state $P^+Q_A^-$ has a shorter lifetime of 100 ms.

In *R. sphaeroides*, the antenna proteins harvest the solar light and funnel excitation energy into the RC where photons are converted into electron-hole couples with a quantum yield close to one [10–12]. The light harvesting role is efficiently played by LH1 and LH2 in the wild type (or strain 2.4.1), but the complexity of the whole system can be diminished without compromising the photosynthetic metabolism. Indeed *R. sphaeroides* strain R26 is mutant lacking one of the light harvesting complex, LH2, and the carotenoid pigments. The R26 mutant grows very efficiently, although using a restricted interval of wavelengths compared to the wild type.

Biohybrids took a bit forward this concept focusing on the pristine RC covalently bound to tailored artificial antennas molecules that act in substitution of the biological LH complexes. The resulting biohybrid systems show a molecular complexity far lower than the photosynthetic apparatus, a higher chemical stability than the LH1-RC non-covalent complex and still efficiently generate electron-hole couples [1,2,5].

Artificial antennas conceived to replace the natural LH complexes must be properly designed and synthesized to fulfill suitable optical required properties. Antennas must have efficient light absorption in the visible range, where the RC does not efficiently absorb, and high emission quantum yield (QY) in correspondence of the RC absorption maxima present in the near infrared (NIR) region (Fig. 1b). High Stokes shift between the antenna absorption and emission spectra is also strongly desirable to prevent the antenna self-absorption and to promote excitation of the RC in a wavelength range where its absorption is limited. Moreover, antennas should be chemically functionalized to be directed and firmly affixed as close as possible to the RC absorbing bacteriochlorophyll pigments. They should have also unhindering chemical structures that do not perturb the protein function.

In our previous work, a biohybrid obtained by covalently linking an organic antenna with aryleneethynylene (AE) structure to the RC was found to have 30% increased photoactivity versus the pristine photoenzyme under white light excitation [4]. This result is a relevant proof of the great potentialities of bioconjugation of organic light harvesting molecules to the RC and it spurs investigation of other classes of organic antennas, with the aim of further improving the efficiencies of charge separation of the biohybrid system under visible light excitation. To this end, here we propose a new antenna molecule (hCyN7) with heptamethine cyanine structure, which has been properly designed and synthesized to be easily anchored to the photoenzyme and to bear optical properties desirable for its function, i.e. absorption and emission peak wavelengths in the visible and NIR region, respectively, large Stokes shift, very high extinction coefficient and fluorescence quantum yield (ε = 60,500, φ_{PL} = 27%) significantly improved if compared to those of the AE molecule (ε = 9760, φ_{PL} = 5.6%). Here we report that, under visible light excitation, the hCyN7-RC biohybrid has 100% increased photoconversion efficiency versus the bare RC.

Besides a careful design of the antenna, clarifying the rate and the mechanism of energy transfer from the antenna to the protein, and the rate of the subsequent charge transfer steps occurring within the protein is also crucial to evaluate, and eventually design, the biohybrid systems suitable for future applications in devices. Ultrafast visible spectroscopy experiments [2] have been successfully applied to investigate the energy transfer and charge separation in biological-

organic biohybrids. In this manuscript we extend the application of ultrafast techniques by measuring time resolved spectra both in the visible and infrared spectral ranges. The use of time resolved visible-pump/IR-probe spectroscopy (TRIR) enables to clearly identify spectral signatures pertaining both to the antenna and to the different RC co-factors, allowing monitoring the dynamics of all the photo-induced processes.

In the following, we thus provide an exhaustive characterization of the spectroscopic properties of the new antenna and the biohybrid system, analysing the picosecond dynamics of the electron-hole couple formation in the photoenzyme with ultrafast visible and IR spectroscopy.

2. Materials and methods

2.1. Chemicals

Lauryl dimethyl *N*-oxide (LDAO, CAS n.1643-20-5) and Triton X-100 (TX-100, CAS n.9002-93-1) were from Fluka. Diethylaminoethyl-Sephacel (DEAE, CAS n. 9013-34-7), all reagents and solvents for the synthesis of cyanine dyes were purchased from Sigma Aldrich at the highest purity degree and used without further purification. Pre-coated TLC-plates RP-18/UV_{254} by Macherey-Nagel Gmbh & Co with silica gel C-18 layer of 0.15 mm and 0.25 mm were used for analytical and preparative TLC, respectively. CombiFlash Rf + chromatograph equipped with a 50 g Gold reverse phase C-18 column was used for hCyN7 purification. High resolution mass spectrometry was carried out by a Shimadzu high performance liquid chromatography-ion trap-time of flight mass spectrometer (LCMS-IT-TOF). FT-IR spectra were recorded using a Perkin–Elmer Spectrum BX spectrophotometer with dry KBr pellets. ^{1}H- and ^{13}C-spectra were recorded at 500 and 125 MHz, respectively, using an Agilent Technologies 500/54 Premium Shielded spectrometer.

2.2. Steady-state spectroscopy

Optical spectra in the range 350–1000 nm were recorded using a Cary 5000 UV-Vis-NIR spectrophotometer (Agilent Technologies Inc. – USA). Steady-state photoluminescence experiments were performed with a FluoroLog (Horiba Jobin-Yvon) spectrofluorometer, using excitation at 650 nm and emission in the range 670–850 nm.

2.3. Transient absorption spectroscopy

2.3.1. Visible transient absorption spectroscopy

The apparatus used for the transient absorption spectroscopy (TAS) measurements is based on a Ti:sapphire regenerative amplifier (BMI Alpha 1000) system pumped by a Ti:sapphire oscillator (Spectra Physics Tsunami). The system produces 100 fs pulses at 785 nm, 1 kHz repetition rate and average power of 450 mW. Excitation pulses at 640 nm have been obtained by pumping a home-made non collinear optical parametric amplifier (NOPA) by a portion of the fundamental 785 nm. The probe pulse was generated by focusing a small portion of the fundamental laser output radiation on a 2 mm thick sapphire window. The pump beam polarization has been set to magic angle with respect to the probe beam by rotating a λ/2 plate. Excitation powers were on the order of 30–50 nJ. Pump-probe delays were introduced by sending the probe beam through a motorized stage. Multichannel detection was achieved by sending the white light continuum after passing through the sample to a flat field monochromator coupled to a home-made CCD detector [http://lens.unifi.it/ew]. TAS measurements were carried out in a quartz cell (2 mm thick) mounted on a movable stage to avoid sample photo degradation and multiple photon excitation.

2.3.2. Transient infrared spectroscopy

The experimental set-up used for time-resolved infrared measurements was based on a Ti:sapphire oscillator/regenerative amplifier, operating at 1 kHz and centered at 800 nm (Legend Elite, Coherent). A portion of the fundamental laser output was split in order to generate the mid-IR probe and the visible pump. The infrared probe had a spectral width of 200 cm^{-1} in the 6 μm region and was obtained by pumping a home built optical parametric amplifier (OPA) with difference frequency generation. The output of the OPA was split into two beams of equal intensity, which were respectively used as probe and reference. The visible pump at 620 nm was generated by pumping a homemade Non Collinear Optical Parametric Amplifier. The pump pulse was attenuated to provide 150 nJ and focused to a spot of ~150 μm in diameter. The polarization of the pump beam was set to the magic angle with respect to the probe beam by rotating a λ\2 plate. A moveable delay line made it possible to increase the time-of-arrival-difference of the pump and probe beams up to 1.5 ns. After the sample, both probe and reference were spectrally dispersed in a spectrometer (TRIAX 180, HORIBA JobinYvon) and imaged separately on a 32 channels double array HgCdTe detector (InfraRed Associated Inc., Florida USA) with a sampling resolution of 6 cm^{-1}. Two spectral windows were separately recorded and then overlapped in order to cover the spectral region 1500–1750 cm^{-1}. The sample was placed in a cell consisting of two CaF_2 windows of 2 mm of thickness, separated by a 100 μm Teflon spacer, which was mounted on a movable stage in order to minimize sample degradation.

2.3.3. Data analysis

In both the visible and infrared spectral ranges, the recorded kinetic traces and transient spectra have been analysed by using a global analysis procedure [15]. The number of kinetic components has been estimated by performing a preliminary singular values decomposition (*SVD*) analysis [16]. Global analysis was performed using the GLOTARAN package (http://glotaran. org) [17], and employing a linear unidirectional “sequential” model.

2.4. Growth of Rhodobacter sphaeroides

The carotenoidless strain *Rhodobacter sphaeroides* R26 was obtained from the Microorganisms and Cell Cultures (DSM n. 2340) and cultivated anaerobically in Siström medium [18,19] under stirring in 1 l screw top flasks. The cultures of the bacteria were deoxygenated by bubbling N_2 gas for 15 min. Tungsten lamps (60 W) provided continuous illumination with an irradiance of about 32 Wm^{-2} on the surface of the vessel. Biomass was collected in the late exponential phase [20,21].

2.5. Isolation of the photosynthetic Reaction Center

The photosynthetic reaction center (RC) was purified according to a previously published procedure [22,23]. The purity ratio (i.e. the ratio of absorbance recorded at 280 nm and 802 nm) was always lower than 1.3. The integrity ratio (the ratio of absorbance recorded at 760 nm and 865 nm) was always around 1. Stock RC solutions were stored in $T_{20}L_{0.025}E_1$ buffer (Tris-HCl 20 mM, EDTA 1 mM, LDAO 0.025%) at pH 8.0. All experiments here reported were performed in $P_{20}E_1T_{0.03}$ buffer (Phosphate 20 mM, EDTA 1 mM, Triton X-100 0.03%) at pH 8.0.

3. Results and discussion

3.1. Synthesis and properties of the organic antenna

The hCyN7 structural design arises from the photophysical properties of its commercial IR-820 precursor (Scheme 1) bearing one chlorine atom bound to the central cyclic core. IR-820 has good solubility and high extinction coefficient in polar protic solvents (Table 1), [24] but is not suitable to function as antenna since its Stokes shift is limited to 37 nm (Table 1). Nevertheless, literature shows that the substitution of

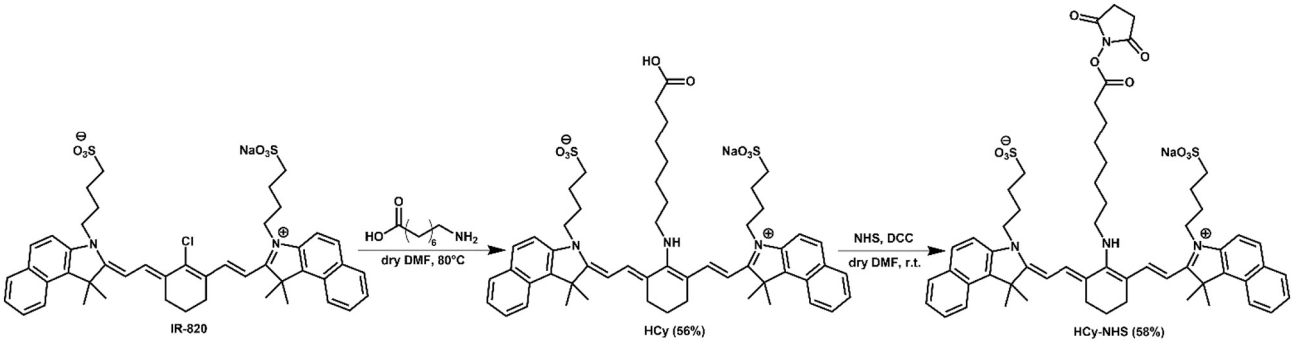

Scheme 1. Synthesis of hCyN7-NHS.

Table 1
Photophysical properties of organic dyes.

Molecule	Solvent	$\lambda_{Abs,max}$ (nm)	$\lambda_{Em,max}$ (nm)	Extinction coefficient[a]	φ_{PL} (%)
IR-820	CH_3OH	820	857	202,000	4.4[b]
hCyN7	$P_{20}E_1TX_{0.03}$	645	800	60,500 ± 300	27[c]
AE800[d]	$T_{20}E_1TX_3$	650	800	9760 ± 60	5.6

[a] $M^{-1}\,cm^{-1}$.
[b] From reference [24].
[c] Using rhodamine 800 as standard.
[d] From reference [4].

the central chlorine atom with an amine moiety leaves the emission spectrum almost unaltered, while it induces significant blue-shift and broadening of the NIR absorption peak, possibly due to an excited-state intramolecular charge transfer between the amino donor and the cyanine acceptor units [25,26]. As a result, the Stokes shift of amino functionalized heptamethine cyanine dyes increases significantly, making this class of molecules very suitable as artificial antennas.

Hence, hCyN7 was synthesized (see details in ESI Section 5) by a straightforward procedure based on the nucleophilic substitution reaction of the chlorine atom in IR-820 with 8-aminooctanoic acid that allows, at the same time, to increase the Stokes shift and insert a carboxyl pendant unit required for bioconjugation. In the second synthetic step, the pendant carboxyl group was converted into succinimidyl ester hCyN7-NHS [27] (Scheme 1), to promote the covalent linking of the antenna to the lysine residues of RC.

This rather simple route, as compared to the synthetic procedures of aryleneethynylene antennas reported in our previous works, leads to a molecular dye fulfilling all the requisites expected for a RC ideal antenna, being (*i*) highly soluble in aqueous media, having (*ii*) high Stokes shift of 155 nm between (*iii*) the intense and broad absorption peak (λ_{max} = 645 nm, ε = 60,500) in the visible region (see optical spectra in Fig. S1), (*iv*) the intense emission peak (λ_{max} = 800 nm) and high quantum yield (φ_{PL} = 27%) in the NIR (see Table 1 and Fig. 1). Moreover, (*v*) the succinimidyl ester binding group enables the bioconjugation chemistry and (*vi*) the long alkyl spacer between this group and the cyanine backbone reduces the sterical hindrance of the dye on the RC surface in proximity of the donor. Details on the synthesis are given in ESI Section 1, and relevant optical spectra are shown in Fig. S1.

The hCyN7 antenna is highly soluble in aqueous buffer but it rapidly degrades under both light and dark conditions (Figs. S2 and S3). Dark and light stabilities are extended by adding a small amount of Triton X-100 detergent (0.03% w/v) (Figs. S4 and S5). This is a clear advantage since, although RC requires mild detergents such as TX-100 to be solubilized in aqueous buffers, the surfactant concentrations should be kept as low as possible to avoid jeopardizing the integrity of the protein.

3.2. Characterization of the hCyN7-RC bioconjugate

The hCyN7-RC hybrid obtained by the bioconjugation of hCyN7-NHS and RC (procedure detailed in ESI Section 3) shows a UV-Vis-NIR absorption spectrum resulting from the combination of the antenna and the protein spectra (Fig. S7). An average of 5.0 ± 0.1 hCyN7 molecules per protein was estimated by spectroscopic analysis using the absorbance at 645 nm of the biohybrid subtracted for the contribution of the native protein (Fig. S7). Moreover, the biohybrid retains the ability to form the photo-induced charge separated state, with amplitude and kinetics similar to that of the native protein treated with the same procedure for bioconjugation without adding the fluorophore (Fig. S8).

The antenna effect was evaluated by measuring the efficiencies of the pristine RC and the biohybrid in generating a photo-induced hole-electron couple $P^+Q_A^-$ that reaches a steady value under continuous illumination. The concentration of $P^+Q_A^-$ can be evaluated spectrophotometrically monitoring the RC absorption dimer peak at 865 nm (Fig. 1) that decreases proportionally to the concentration of the charge separated state with $\Delta\varepsilon = 105\,mM^{-1}\,cm^{-1}$.

As expected, the antenna is ineffective upon illumination at 800 nm, where it has very low spectral contributions compared to the RC (Fig. S9A). On the contrary, when illuminating at the maximum hCyN7 absorption wavelength (645 nm) where the RC absorption is negligible, the $P^+Q_A^-$ concentration produced in the hybrid system is 3.7 ± 0.1 times higher than that in the native RC (Fig. S9B), an enhancement comparable to that of AE800. Noteworthy, irradiating the hCyN7-RC bioconjugate with visible light in the 380–668 nm interval, the $P^+Q_A^-$ concentration is doubled versus the pristine protein *i.e.* the overall photoactivity increases to the unmatched value of 100 ± 3% (Fig. 2).

Being a photoenzyme, RC catalyzes, within the bacterial photosynthetic membrane, the transfer of two electrons from the cytochrome

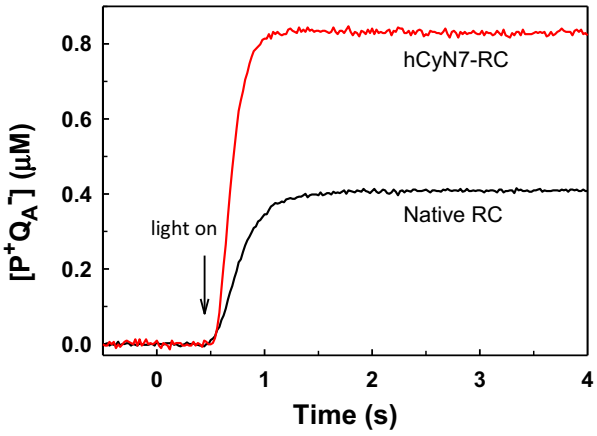

Fig. 2. Amount of charge separated state obtained for the native RC and the hCyN7-RC bioconjugate under white light (380–668 nm) illumination.

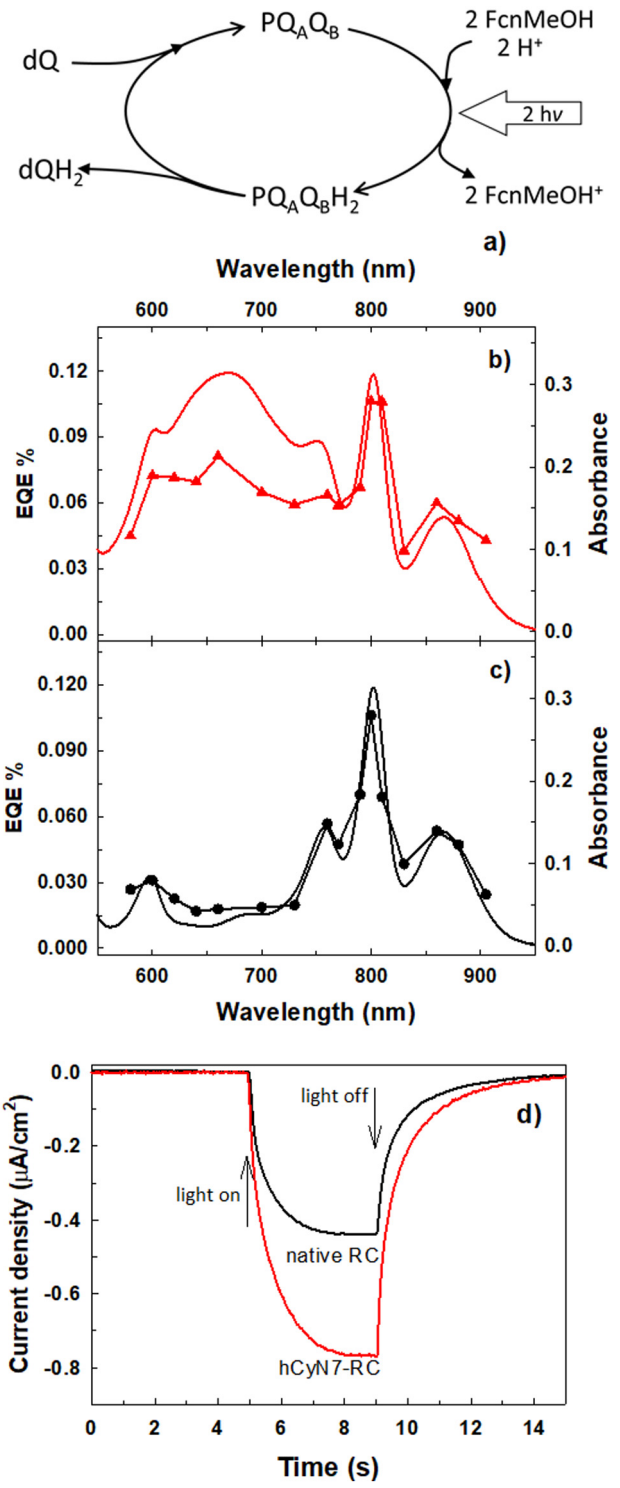

Fig. 3. a) The photocycle of the bacterial reaction center. P: dimer, Q_A: quinone sitting in the primary binding site, Q_B: quinone sitting in the secondary binding site, FcnMeOH and $FcnMeOH^+$: reduced and oxidized form of the synthetic electron donor, dQ: unbound decylubiquinone, dQH_2: unbound decylubiquinole. b, c) hCyN7-RC (red) and RC (black) spectra superimposed to the corresponding action spectra (triangles and circles). d. Photocurrent enhancement associated to the use of hCyN7 as antenna. The exciting light is in the interval 380–668 nm to a phosphate 90 mM, TX-100 0.03% pH 7.0 solution of RC or hCyN7-RC. (For interpretation of the references to colour in this figure legend, the reader is referred to the web version of this article.)

c_2 to the final electron acceptor, the quinone sitting in the Q_B-binding site, eventually producing one molecule of quinole every two absorbed photons. Such reaction is cyclic and can be sustained by light as long as the exogenous quinone and the reduced cytochrome c_2 are available. It is also possible to perform the photocycle in aqueous solution using for instance the electron acceptor decylubiquinone (dQ) and the electron donor ferrocenemethanol (FcnMeOH) which efficiently substitute (Fig. 3a) ubiquinol and cytochrome c_2. The quinone reduction:

$2FcnMeOH + dQ + 2H^+ \overset{RC,h\nu}{\rightarrow} 2FcnMeOH^+ + dQH_2$ can be photodriven in a three-electrode configuration photoelectrochemical cell. The current generated upon light irradiation, under the open circuit voltage (OCV), has been recorded for both the pristine and biohybrid solutions.

Driving the photocycle by illuminating at the maximum hCyN7 absorption wavelength (645 nm), a remarkable 3.5-fold increase in the photocurrent was observed for hCyN7-RC vs RC, in good agreement with the 3.7-fold enhanced concentration of charge-separated state (Fig. S10).

Photocurrents were also measured upon excitation of both RC and hCyN7-RC solutions with different wavelengths ranging from 580 to 910 nm, using a set of 10 nm bandpass interferential filters. The photoenzyme action spectra (Fig. 3b, c) were then obtained by plotting the external quantum efficiency versus the excitation wavelengths (see SI for more details). The data are compared with the corresponding optical spectra represented by the continuous line. In the case of pristine RC, photocurrents satisfactorily match the absorption peaks of the protein over the entire spectrum with the maximum value at 800 nm, in correspondence of the maximum absorption (see SI5).

The action spectrum of the hCyN7-RC bioconjugate shows the same satisfactory match in the NIR region characterized by the presence of the protein absorptions, while a slight mismatch between absorption cross-section and EQE (EQEs are about 30% less than the value expected from the absorption spectrum) appears in the 550–750 nm interval (Fig. 3b). This is not surprising as a portion of the hCyN7 antenna effect could be wasted by several factors including the emission spectrum that does not overlap completely with the NIR absorption peaks of RC (Fig. 1) or the possibility that the antenna collects energy but is not able to transfer to RCs which are already in their charge-separated state. Despite these energetic losses, the gain in the hCyN7-RC vs RC photocurrents still ranges from 3 to 3.5 in the entire interval 550–750 nm.

In a further experiment shown in Fig. 3d, photocurrents were recorded under illumination with white light (380–668 nm). Photocurrent generated by hCyN7-RC was found to be 75 ± 6% higher than that from RC, this being a remarkable increase although lower than that observed for the concentration of charge-separated state (100%, Fig. 2). This result is again not unexpected considering that the charge separated state generation is only one of the several steps leading to photocurrent, and charge separated states can disappear via secondary reactions and other dissipative paths.

The Förster radius and the FRET efficiencies calculated for hCyN7 are given in section 3A of ESI (see tables S3A.1, S3A.2 and S3A.3). FRET efficiencies calculation is limited to the nine lysine residues in close proximity of the detergent toroid surrounding the RC, i.e. L268, L82, M110, M144, H62, H197, H60, L204 and L202. The value of R_0 = 7.9 nm and the length of the pendant in hCyN7 make the FRET efficiency in the biohybrid system always higher than 84% even in the most unfavorable case.

3.3. Ultrafast transient absorption spectroscopy

Having shown that hCyN7 is able to act as an antenna and that the amount of energy transferred to the RC is not residual, we settled to retrieve the time constant of energy transfer between hCyN7 and RC, and to investigate the effect of bioconjugation on the following charge

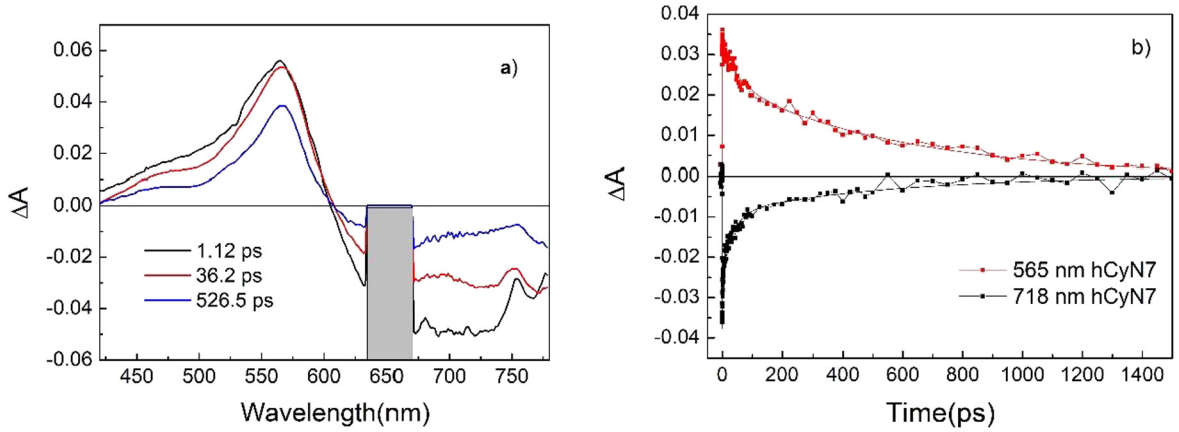

Fig. 4. a) EADS obtained from global analysis of TAS spectra of hCyN7, recorded upon excitation at 645 nm; b) kinetic traces registered at the 565 nm (red trace) and 718 nm (black trace) for hCyN7. Continuous lines are fits retrieved from global analysis. (For interpretation of the references to colour in this figure legend, the reader is referred to the web version of this article.)

separation dynamics by sub-picosecond transient absorption spectroscopy (TAS) in the visible spectral range.

Preliminary measurements were performed in order to investigate the photodynamic behavior of the isolated antenna. The transient absorption spectra measured for hCyN7 in buffer solution upon excitation at 640 nm show a broad Excited State Absorption (ESA) band peaking at 565 nm and a bleaching/stimulated emission band extending over 750 nm. To extract the time constants describing the dynamic evolution of the system upon photoexcitation, the recorded transient data have been fitted using global analysis [15] employing a sequential kinetic scheme with increasing lifetimes. This fitting procedure allows the simultaneous fit of the kinetic traces measured at all the probe wavelengths with combination of exponential functions. As a result it retrieves the kinetic constants representative for the system evolution and the corresponding spectral components, named as Evolution Associated Difference Spectra (EADS), which evidence the most significant spectral changes occurring for each determined time constant. In case of our system three kinetic components were necessary to accurately fit the data, retrieving the EADS reported in Fig. 4a. In the same figure (panel b) two representative kinetic traces, with the corresponding fit are also shown.

Previous investigations of other heptamethine cyanine dyes, all bearing an amine group coordinated to the central carbon atom of the cyanine structure, as occurring also for hCyN7 [26,28] have shown that an intramolecular charge transfer (ICT) process is likely to occur upon photoexcitation. In particular, it has been shown that light absorption induces the population of a local excited state (LE), which then rapidly relaxes towards an ICT state, where the electronic density shifts towards the central amine functionality of the molecule. The occurrence of photoinduced ICT well accounts for the large fluorescence Stokes shift observed for heptamethine cyanine dyes with an amine present on the chain instead than a chlorine atom (as it happens in case of hCyN7 if compared with the IR-820 precursor), and for the lack of mirror image symmetry between absorption and fluorescence spectra, which can be ascribed to a molecular geometry change accompanying the transition between the LE and ICT state.

In case of hCyN7, the EADS shown in Fig. 4a indicate the presence of a fast kinetic component, possibly associated to the transition between the LE and ICT states, a slower relaxation process occurring in about 36 ps and the recovering of the ground state in about 525 ps. To better characterize the dynamic of the LE → ICT transition, which is expected to be associated to a conformational change of the molecule, we also measured transient absorption spectra in the midIR range. Time resolved IR spectra (TRIR) at several pump-probe delays and the corresponding EADS obtained from global analysis are reported in Fig. 5.

The first kinetic component retrieved from global analysis shows several negative signals due to the bleaching of ground state vibrations in the 1300–1650 cm^{-1} region, likely attributable to C=C stretching, ring modes and carbonyl stretching modes, together with the corresponding ESA bands. The intensity of the ESA bands mostly decays on a fast 0.7 ps timescale (evolution from the black to red component in Fig. 5b), indicating vibrational cooling in the excited state. On the same timescale, however, the molecule also undergoes a conformational change, as demonstrated for instance by the disappearance of the small bleaching signal at 1530 cm^{-1} and the intensification of the negative signal at 1555 cm^{-1} (mostly due to the decay of the broad ESA signal around 1604 cm^{-1}). The occurrence of a conformational change, mostly involving the region of the C=C stretching and ring mode vibrations, allows to associate the fast kinetic component to the relaxation between the LE and ICT state. The following kinetic component, with a 23.3 ps lifetime can be interpreted in terms of a relaxation of the ICT state, possibly induced by the rearrangement of the solvent molecules. Finally, return to the ground state occurs on the nanosecond timescale. The slight difference in the lifetimes observed between measurements performed in the visible and IR spectral range is ascribed to the different solvent used for the two experiments (respectively PET buffer and methanol).

To evaluate the dynamics of energy transfer and charge separation, the transient absorption spectra of the hCyN7-RC biohybrid were then measured and compared to those of the isolated antenna. In the visible spectral range, transient absorption spectra of hCyN7 and hCyN7-RC are apparently very similar, as shown in Fig. 6, where the EADS resulting from global analysis of TAS data recorded for hCyN7-RC and the comparison of significant kinetic traces recorded for hCyN7 and the hCyN7-RC are reported. For hCyN7-RC, TAS data have been fitted using four kinetic components: although a quite satisfactory fit could also be obtained using three kinetic components, the addition of a further time constant significantly improves the fit at the long timescale.

As shown by comparing the EADS reported in Figs. 4 and 6, the transient spectra of both hCyN7 and hCyN7-RC are dominated by the dye absorption features, thus preventing a straightforward evaluation of the kinetics of the electron transfer steps occurring in the RC. The excited states evolution of the two systems is however different, showing a faster recovering of the transient signals in case of hCyN7-RC, due to the occurrence of energy transfer from the hCyN7 antenna towards the RC, as noticed from the comparison of the kinetic traces shown in Fig. 6b and c. In particular the ESA band significantly decays on the 9.6 ps timescale and further decays on the 121 ps timescale (black to red evolution in Fig. 6a). The precise assignment of the observed spectral evolution to specific electron transfer step is however difficult, since the most intense absorptions of the RC pigments are at wavelengths > 800 nm, a spectral range which is not covered in our

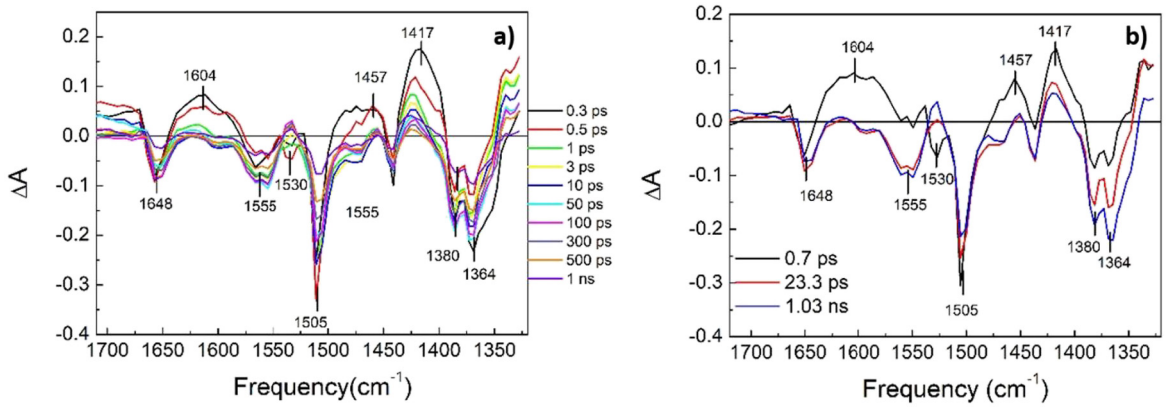

Fig. 5. a) TRIR spectra of hCyN7 in methanol, recorded upon excitation at 620 nm; b) EADS obtained from global analysis of the time resolved spectra shown in panel a).

measurement.

A more detailed picture of the charge separation dynamics can be obtained by recurring to ultrafast Vis-pump/IR-probe spectroscopy. The dynamics of all the electron transfer steps occurring in pristine RCs has been widely investigated using steady state FTIR spectroscopy and ultrafast time resolved IR techniques, allowing a robust assignment of the spectral signatures identifying the different radical pairs resulting from the subsequent steps of charge separation [29–31]. The comparison of the TRIR spectra of hCyN7 and hCyN7-RC provides a tool to disentangle spectral signatures pertaining to the antenna and the RC chromophores, elucidating the kinetics of both energy transfer from hCyN7 to the RC and of the following electron transfer steps.

The TRIR spectra of hCyN7-RC have been recorded using a broadband excitation pulse centered at 620 nm, to maximize the antenna absorption and reduce direct RC excitation.

Fig. 7a reports the EADS obtained by fitting the TRIR spectra of hCyN7-RC with global analysis, using a sequential decay scheme with four kinetic constants (difference spectra at selected pump-probe delays are shown in Fig. S11). A collection of selected kinetic traces is shown in Fig. 7b. Time constants obtained fitting the TRIR data are in close agreement with those obtained from the TAS data.

The initial spectral component (black line in Fig. 7a), with 1 ps lifetime, shows several bleaching signals, at 1505, 1528 and 1545 cm^{-1}, as well as a broad absorption in the 1608 cm^{-1} region

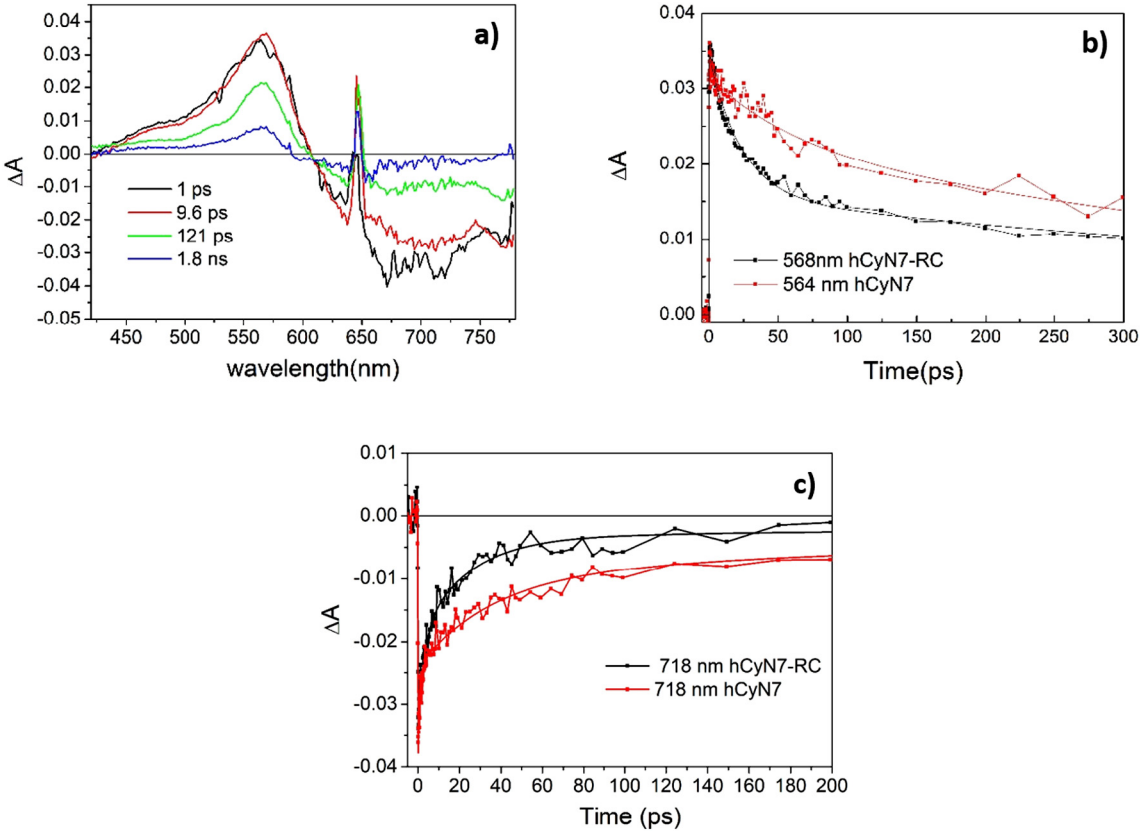

Fig. 6. a) EADS obtained from global analysis of TAS spectra of hCyN7-RC, recorded upon excitation at 645 nm; b) comparison of the kinetic traces registered at the maximum of the ESA band for hCyN7 (red trace) and hCyN7-RC (black trace); c) comparison of the kinetic traces registered at the bleaching/stimulated emission band for hCyN7 (red trace) and hCyN7-RC (black trace). Continuous lines are fits retrieved from global analysis. (For interpretation of the references to colour in this figure legend, the reader is referred to the web version of this article.)

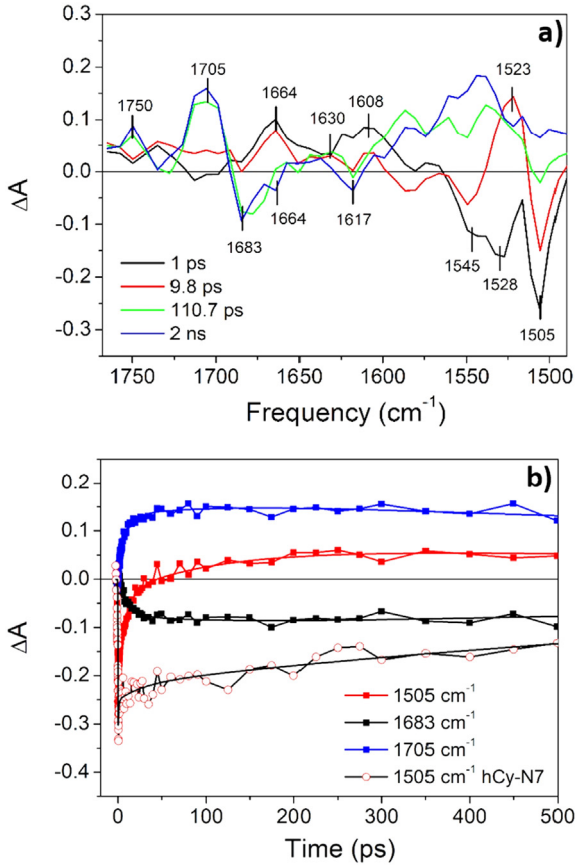

Fig. 7. a) EADS obtained by global analysis of TRIR spectra of the hCyN7-RC biohybrid, recorded upon excitation at 620 nm; b) selected kinetic traces, corresponding to the recovery of hCyN7 bleaching (1505 cm^{-1}), bleaching of the 9-keto carbonyl of the P bacteriochlorophylls (1683 cm^{-1}); rise of the P^+ 9-keto carbonyl absorption (1705 cm^{-1}). The kinetic trace at 1505 cm^{-1} registered for the hCyN7 in solution is shown for comparison (red circles). Squares are experimental points, continuous lines are fits retrieved from global analysis. (For interpretation of the references to colour in this figure legend, the reader is referred to the web version of this article.)

which can be attributed to hCyN7, since those signals are also present in the TRIR spectra of the isolated antenna chromophore (see Fig. 5). The positive band at 1664 cm^{-1}, which is not observed for the dye in solution, could represent a protein response following light absorption from the pigment, being in the region characteristic for amide I absorption [32]. In the second spectral component (red line in Fig. 5a) hCyN7 bleaching signals partially recover, whereas new absorption bands develop, such as the one peaked at 1523 cm^{-1} or the broad low intensity feature at 1690–1720 cm^{-1}. The recovery of the negative signal at 1528 cm^{-1} and the simultaneous rise of the peak at 1523 cm^{-1}, as well as the decrease in intensity of the broad band at 1608 cm^{-1} well correspond to the evolution observed on the fast timescale for the isolated dye in solution and assigned to LE → ICT transition of hCyN7 (note that in methanol solution a peak at 1530 cm^{-1} rises on the 0.7 ps timescale, frequency shifts can be due to the different environment in which the dye is located). Apparently thus, coordination to the RC does not perturb the excited state evolution of the dye on the fast timescale, with the relaxation to the ICT state still occurring also in close proximity to the protein. Comparison with literature data [30], reported in SI (Fig. S12) demonstrates that besides the initial spectral component, TRIR data acquired for the bio-hybrid and for the bare RC are very similar, indicating that, once the energy has reached the electron donors in the protein, charge separation leads to the formation of the same radical pairs in both samples. This comparison furthermore indicates that some signals observed in the initial spectral component could also be assigned to the RC excited state, with the excitation energy mainly localized on the special pair P. A distinctive feature indicating population of P* is indeed a broad and low intensity absorption around 1700 cm^{-1}, similar to that observed in our spectra. This finding would suggest the occurrence of a fast 1 ps energy transfer component from the LE state of hCyN7 to the RC or a partial direct excitation of the reaction center at the excitation wavelength used in our measurement. Indeed TRIR data, reported in reference 30 for the isolated RC have been collected upon excitation at 600 nm. Inspection of the kinetic traces associated to the bleaching of hCyN7 modes, as the one at 1505 cm^{-1}, shows that the signal significantly recovers on a *ca* 10 ps time scale. On this same timescale the characteristic differential band pattern assigned to the formation of the $P^+H_A^-$ radical pair, extensively characterized through FTIR spectroscopy [see [29] and articles cited therein] can be clearly identified (Fig. 7 green line; see also the kinetic traces reported in panel b). Spectral signatures attributed to such radical pair are in fact the negative peak at 1683 cm^{-1} due to the bleaching of the 9-keto carbonyl group of the special pair, which upshifts upon oxidation to 1705 cm^{-1}, as well as the positive signal at 1750 cm^{-1}, due to the absorption of the 10-ester carbonyl group of P^+ [29–31]. The spectral signatures in the 1640–1617 cm^{-1} range have been interpreted in terms of H_A^- formation ad mostly assigned to a protein conformational change following the bacteriopheophytin reduction [30]. The evolution occurring on the 9.8 ps timescale can be thus interpreted in terms of energy transfer from the artificial antenna dye towards the RC, and subsequent formation of the $P^+H_A^-$ radical pair. Since the LE → ICT relaxation of hCyN7 is observed on a 1 ps timescale, we conclude that energy transfer towards the RC pigments mostly occurs from the charge transfer state of the antenna.

In native RCs, upon direct excitation of the special pair, the initial electron transfer step producing $P^+H_A^-$ occurs on a 3 ps timescale [33], which is shorter than timescale here observed for the energy transfer from hCyN7 (*ca* 10 ps). This implies that in our system the excited state of the RC is not accumulated, since it is depopulated faster than as it is formed. For this reason it is difficult to establish which particular chromophore would receive energy from the antenna. Most probably, since the biohybrid contains on average 5 pigments per RC and the fluorescence from the antenna well overlaps with the absorption of all the bacteriochlorophylls and the bacteriopheophytins linked to the protein, energy will be transferred to both the special pair P and the to the neighbor monomer bacteriochlorophylls and possibly also to the bacteriopheophytins. Energy equilibration among the RC pigments has been shown to be very fast [34,35], and it is not resolved in our measurements. On the other hand, the spectral evolution occurring on the following 110 ps timescale, and associated to the rise of the last spectral component (green to blue evolution in Fig. 7a), can be interpreted in terms of electron transfer from the bacteriopheophytin towards Q_A. One of the distinctive features signaling the arrival of the electron on Q_A is the development of the negative signal at 1664 cm^{-1}, assigned to a change of the amide I transition in response to electron transfer [30,36]. Comparison with previously reported data for the native RCs suggests the electron transfer from the bacteriopheophytin to Q_A being faster in hCyN7-RC, since a *ca* 220 ps rate is usually reported for the native system [30,37]. Considering that energy equilibration among all the bacteriochlorophylls and bacteriopheophytins occurs on a sub-ps timescale [34,35,38] the kinetics of secondary charge separation should not depend on the initial excitation conditions. The exact reason for the observed acceleration of the electron transfer towards Q_A is difficult to disentangle from the currently available data, but it is consistently observed in both our visible pump-probe and TRIR data. A control transient absorption measurement, executed on the bare RC using the same buffer and detergent employed for the bioconjugate, furthermore suggests that the sample treatment does not influence the kinetics of Q_A reduction, since in that case the usual ~220 ps rate is retrieved (Fig.

S13).

4. Conclusions

The results described in this work indicate that a careful design of artificial antenna dyes, aimed at optimizing their optical properties in way to meet the criteria ensuring efficient energy transfer towards the photosynthetic reaction center, allows to construct biohybrid systems with doubled photoactivity under visible light excitation as compared to the pristine photoenzyme. Pump probe experiments performed both in the visible and IR spectral range allowed to elucidate the rate of energy transfer from the artificial antenna to the protein, and of the subsequent intra-protein charge transfer processes. Our results show that the energy transfer from the organic antenna to the reaction center is very efficient and fast, as confirmed by the strong reduction of the excited state lifetime of hCyN7 when it is linked to the protein versus the hCyN7 free molecule. Moreover, we show that all the electron transfer steps naturally occurring in the pristine protein are operative and preserved, demonstrating that the introduction of the artificial antenna does not perturb the protein structure and its operation.

Author information

The authors declare no competing financial interests.

Transparency document

The Transparency document associated with this article can be found, in online version.

Acknowledgments

Massimo Dell'Edera is acknowledged for his help in the synthesis of hCyN7. This work was financed by Università degli Studi “Aldo Moro” di Bari, Italy (IDEA 2011 project “BIOEXTEND: Extending enzymatic properties by bioconjugation of enzymes with fluorescent organic oligomers”) and by the Apulia Region, Italy funded (Project “FONTANAPULIA – FOtocatalizzatori NanosTrutturati e rAdiazioNe UV per un'Acqua più PULItA” Project n. WOBV6K5).

Appendix A. Supplementary data

Data relative to: the chemicals used, the procedures for bacteria growth and RC isolation, the synthesis of the organic antenna, the study of its (photo) stability, the bioconjugation procedure, the calculation of Förster distance and FRET efficiency, the study of photoexcitation and photocurrent generation of the bioconjugate system, the energy transfer efficiency calculation, the experiments of ultrafast visible and infrared spectroscopy (Word document). Supplementary data to this article can be found online at https://doi.org/10.1016/j.bbabio.2019.01.009.

References

[1] F. Milano, R.R. Tangorra, O. Hassan Omar, R. Ragni, A. Operamolla, A. Agostiano, G.M. Farinola, M. Trotta, Enhancing the light harvesting capability of a photosynthetic reaction center by a tailored molecular fluorophore, Angew. Chem. 124 (2012) 11181–11185.
[2] P.K. Dutta, S. Lin, A. Loskutov, S. Levenberg, D. Jun, R. Saer, J.T. Beatty, Y. Liu, H. Yan, N.W. Woodbury, Reengineering the optical absorption cross-section of photosynthetic reaction centers, J. Am. Chem. Soc. 136 (2014) 4599–4604.
[3] P.K. Dutta, S. Levenberg, A. Loskutov, D. Jun, R. Saer, J.T. Beatty, S. Lin, Y. Liu, N.W. Woodbury, H. Yan, A DNA-directed light-harvesting/reaction center system, J. Am. Chem. Soc. 136 (2014) 16618–16625.
[4] O. Hassan Omar, S. la Gatta, R.R. Tangorra, F. Milano, R. Ragni, A. Operamolla, R. Argazzi, C. Chiorboli, A. Agostiano, M. Trotta, G.M. Farinola, Synthetic antenna functioning as light harvester in the whole visible region for enhanced hybrid photosynthetic reaction centers, Bioconjug. Chem. 27 (2016) 1614–1623.
[5] P.I. Gordiichuk, D. Rimmerman, A. Paul, D.A. Gautier, A. Gruszka, M. Saller, J.W. de Vries, G.J. Wetzelaer, M. Manca, W. Gomulya, M. Matmor, E. Gloukhikh, M. Loznik, N. Ashkenasy, P.W. Blom, M. Rogner, M.A. Loi, S. Richter, A. Herrmann, Filling the green gap of a megadalton photosystem I complex by conjugation of organic dyes, Bioconjug. Chem. 27 (2016) 36–41.
[6] S. la Gatta, O. Hassan Omar, A. Agostiano, F. Milano, R.R. Tangorra, A. Operamolla, C. Chiorboli, R. Argazzi, M. Natali, M. Trotta, G.M. Farinola, R. Ragni, A far-red emitting aryleneethynylene fluorophore used as light harvesting antenna in hybrid assembly with the photosynthetic reaction center, MRS Adv. 1 (7) (2016) 495–500.
[7] S. Bahatyrova, R.N. Frese, C.A. Siebert, J.D. Olsen, K.O. van der Werf, R. van Grondelle, R.A. Niederman, P.A. Bullough, C. Otto, C.N. Hunter, The native architecture of a photosynthetic membrane, Nature 430 (2004) 1058–1062.
[8] G. Feher, J.P. Allen, M.Y. Okamura, D.C. Rees, Structure and function of bacterial photosynthetic reaction centres, Nature 339 (1989) 111–116.
[9] F. Mavelli, M. Trotta, F. Ciriaco, A. Agostiano, L. Giotta, F. Italiano, F. Milano, The binding of quinone to the photosynthetic reaction centers: kinetics and thermodynamics of reactions occurring at the Q_B^- site in zwitterionic and anionic liposomes, Eur. Biophys. J. (2014) 1–15.
[10] A. Operamolla, R. Ragni, F. Milano, R.R. Tangorra, A. Antonucci, A. Agostiano, M. Trotta, G.M. Farinola, “Garnishing” the photosynthetic bacterial reaction center for bioelectronics, J. Mater. Chem. C 3 (2015) 6471–6478.
[11] R.R. Tangorra, A. Antonucci, F. Milano, S. la Gatta, G.M. Farinola, A. Agostiano, R. Ragni, M. Trotta, Hybrid interfaces for electron and energy transfer based on photosynthetic proteins, in: M. Pessarakli (Ed.), Handbook of Photosynthesis, Third edition, CRC Press, USA, 2016, pp. 201–220.
[12] F. Milano, R.R. Tangorra, A. Agostiano, L. Giotta, V. De Leo, F. Ciriaco, M. Trotta, Modulating the lifetime of the charge-separated state in photosynthetic reaction center by out-of-protein electrostatics, MRS Adv. 3 (27) (2018) 1497–1507.
[13] B.D. Belviso, R.R. Tangorra, F. Milano, O. Hassan Omar, S. la Gatta, R. Ragni, A. Agostiano, G.M. Farinola, R. Caliandro, M. Trotta, Crystallographic analysis of the photosynthetic reaction center from *Rhodobacter sphaeroides* bioconjugated with an artificial antenna, MRS Adv. 1 (57) (2016) 3789–3800.
[14] M.H.B. Stowell, T.M. McPhillips, D.C. Rees, S.M. Soltis, E. Abresch, G. Feher, Light-induced structural changes in photosynthetic reaction center: implications for mechanism of electron-proton transfer, Science 276 (1997) 812–816.
[15] I.H.M. van Stokkum, D.S. Larsen, R. van Grondelle, Global and target analysis of time-resolved spectra, Biochim. Biophys. Acta 1657 (2004) 82–104.
[16] E.R. Henry, J. Hofrichter, Singular value decomposition: application to analysis of experimental data, in: M.L.J. Ludwig Brand (Ed.), Numerical Computer Methods, Academic Press, 1992, pp. 129–192.
[17] J.J. Snellenburg, S. Laptenok, R. Seger, K.M. Mullen, I.H.M. van Stokkum, Glotaran: a java-based graphical user interface for the R package TIMP, J. Stat. Softw. vol 1, (Issue 3) (2012).
[18] W.R. Sistrom, The kinetics of the synthesis of photopigments in *Rhodopseudomonas spheroides*, J. Gen. Microbiol. 28 (1962) 607–616.
[19] W.R. Sistrom, Observations on the relationship between the formation of photopigments and the synthesis of protein in *Rhodopseudomonas spheroides*, J. Gen. Microbiol. 28 (1962) 599–605.
[20] F. Italiano, A. Buccolieri, L. Giotta, A. Agostiano, L. Valli, F. Milano, M. Trotta, Response of the carotenoidless mutant *Rhodobacter sphaeroides* growing cells to cobalt and nickel exposure, Int. Biodeterior. Biodegrad. 63 (2009) 948–957.
[21] E. Asztalos, F. Italiano, F. Milano, P. Maroti, M. Trotta, Early detection of mercury contamination by fluorescence induction of photosynthetic bacteria, Photochem. Photobiol. Sci. 9 (2010) 1218–1223.
[22] F. Milano, F. Italiano, A. Agostiano, M. Trotta, Characterisation of RC-proteoliposomes at different RC/lipid ratios, Photosynth. Res. 100 (2009) 107–112.
[23] F.M. Emiliano Altamura, Francesco Milano, Massimo Trotta, Photosynthesis without the organisms: the bacterial chromatophores, in: F.R. Stefano Piotto, Simona Concilio, Ernesto Reverchon, Giuseppe Cattaneo (Eds.), Advances in Bionanomaterials, 177 Springer International Publishing, 2017(pp. X).
[24] N.S. James, Y. Chen, P. Joshi, T.Y. Ohulchanskyy, M. Ethirajan, M. Henary, L. Strekowsk, R.K. Pandey, Evaluation of polymethine dyes as potential probes for near infrared fluorescence imaging of tumors: part - 1, Theranostics 3 (2013) 692–702.
[25] W. Pham, L. Cassell, A. Gillman, D. Koktysh, J.C. Gore, A near-infrared dye for multichannel imaging, Chem. Commun. (2008) 1895–1897.
[26] X. Peng, F. Song, E. Lu, Y. Wang, W. Zhou, J. Fan, Y. Gao, Heptamethine cyanine dyes with a large stokes shift and strong fluorescence: a paradigm for excited-state intramolecular charge transfer, J. Am. Chem. Soc. 127 (2005) 4170–4171.
[27] R.P. Johnson, Y.I. Jeong, J.V. John, C.W. Chung, S.H. Choi, S.Y. Song, D.H. Kang, H. Suh, I. Kim, Lipo-poly(L-histidine) hybrid materials with pH-sensitivity, intracellular delivery efficiency, and intrinsic targetability to cancer cells, Macromol. Rapid Commun. 35 (2014) 888–894.
[28] L.-C. Zhou, G.-J. Zhao, J.-F. Liu, K.-L. Han, Y.-K. Wu, X.-J. Peng, M.-T. Sun, The charge transfer mechanism and spectral properties of a near-infrared heptamethine cyanine dye in alcoholic and aprotic solvents, J. Photochem. Photobiol. A Chem. 187 (2007) 305–310.
[29] A. Mezzetti, W. Leibl, Time-resolved infrared spectroscopy in the study of photosynthetic systems, Photosynth. Res. 131 (2017) 121–144.
[30] N.P. Pawlowicz, R. van Grondelle, I.H.M. van Stokkum, J. Breton, M.R. Jones, M.L. Groot, Identification of the first steps in charge separation in bacterial photosynthetic reaction centers of *Rhodobacter sphaeroides* by ultrafast mid-infrared spectroscopy: electron transfer and protein dynamics, Biophys. J. 95 (2008) 1268–1284.
[31] M. Di Donato, M.L. Groot, Ultrafast infrared spectroscopy in photosynthesis, Biochim. Biophys. Acta 1847 (2015) 2–11.
[32] P. Hamm, M. Lim, R.M. Hochstrasser, Structure of the amide I band of peptides measured by femtosecond nonlinear-infrared spectroscopy, J. Phys. Chem. B 102

(1998) 6123–6138.
[33] C. Kirmaier, D. Holten, Primary photochemistry of reaction centers from the photosynthetic purple bacteria, Photosynth. Res. 13 (1987) 225–260.
[34] E. Romero, R. Augulis, V.I. Novoderezhkin, M. Ferretti, J. Thieme, D. Zigmantas, R. van Grondelle, Quantum coherence in photosynthesis for efficient solar-energy conversion, Nat. Phys. 10 (2014) 676.
[35] A. Niedringhaus, V.R. Policht, R. Sechrist, A. Konar, P.D. Laible, D.F. Bocian, D. Holten, C. Kirmaier, J.P. Ogilvie, Primary processes in the bacterial reaction center probed by two-dimensional electronic spectroscopy, Proc. Natl. Acad. Sci. 115 (2018) 3563.
[36] S. Maiti, B.R. Cowen, R. Diller, M. Iannone, C.C. Moser, P.L. Dutton, R.M. Hochstrasser, Picosecond infrared studies of the dynamics of the photosynthetic reaction center, Proc. Natl. Acad. Sci. 90 (1993) 5247.
[37] P.N. Dominguez, M. Himmelstoss, J. Michelmann, F.T. Lehner, A.T. Gardiner, R.J. Cogdell, W. Zinth, Primary reactions in photosynthetic reaction centers of *Rhodobacter sphaeroides* – time constants of the initial electron transfer, Chem. Phys. Lett. 601 (2014) 103–109.
[38] S. Westenhoff, D. Palecek, P. Edlund, P. Smith, D. Zigmantas, Coherent picosecond exciton dynamics in a photosynthetic reaction center, J. Am. Chem. Soc. 134 (2012) 16484–16487.